



GEOQuébec
2015

*Challenges from North to South
Des défis du Nord au Sud*

X-ray CT Observation on the Light Backfill

Grytan Sarkar & Sumi Siddiqua

School of Engineering – University of British Columbia, Kelowna, BC,
Canada

ABSTRACT

Swelling pressure and hydraulic conductivity of light backfill (LBF) largely depends on its microstructure as well as the pore space geometry. The microstructural behaviour of the LBF samples was investigated using Xradia Micro XCT-400. The X-ray source, detector, and a small portion of LBF specimen were placed closely to acquire a good quality image with a voxel size of $1.15 \times 1.15 \times 1.15 \mu\text{m}$. The scanned images were de-noised and segmented to study the pore space geometry. An algorithm was developed to compute the volume porosity and pore-size distribution of the scanned samples. Additionally, the interconnected pore components and absolute permeability of the LBF samples were analyzed using Avizo software. The results of microstructure analysis demonstrate that the porosity, pore size and volume of interconnected pores of LBF samples are very low compared to the dry materials. Similarly, the hydraulic conductivity of the LBF samples found from the Avizo Xlab simulation was very low due to the formation of DDL.

RÉSUMÉ

La pression de gonflement et la conductivité hydraulique d'un remblai léger (LBF) dépendent largement de sa microstructure et de la géométrie de l'espace poreux. Le comportement de la microstructure des échantillons de LBF a été étudié en utilisant Xradia Micro XCT-400. La source du rayon X, le détecteur, et une petite partie de l'échantillon de LBF ont été placés étroitement pour acquérir une image de bonne qualité avec une taille de voxel de $1,15 \times 1,15 \times 1,15$ microns. Les images numérisées ont été segmentées pour étudier la géométrie de l'espace poreux. Un algorithme a été développé pour calculer la distribution de la porosité volumique et la taille des pores des échantillons numérisés. En outre, les composants interconnectés des pores et la perméabilité absolue des échantillons de LBF ont été analysés en utilisant le logiciel Avizo. Les résultats de l'analyse de la microstructure ont montré que la porosité, la taille et le volume des pores interconnectés des échantillons de LBF sont très faibles par rapport à la matière sèche. De même, la conductivité hydraulique des échantillons de LBF trouvée avec la simulation Avizo Xlab était très faible en raison de la formation de DDL.

1 INTRODUCTION

Radioactive waste in Canada is mainly originated from nuclear power reactor to produce electricity. Although electricity of this country is mainly produced from hydroelectric power and stream reactor but only 16 % of the total electricity is produced from the nuclear power reactor (Statistics Canada, 2013). However, the rate of generation of radioactive waste in Canada is increasing in every year and stored in large canisters on the surface for the final disposal (International Nuclear Societies Council, 2012). It is a great concern to dispose this waste in a safest place for thousands of years. The deep geological repositories (DGR) concept is a quite new and acceptable technique for the safe disposal of radioactive waste, where wastes are disposed to a depth of 500 to 750 m below the ground surface. Moreover, the addition of Canadian engineered multi barrier concept, which includes highly compacted bentonite (HCB), bentonite-Sand Buffer (BSB), dense Backfill (DBF), Light Backfill (LBF) and Gap Fill (GF) improves the DGR technique to a great extent (Baumgartner et al., 2008; Siddiqua et al., 2011).

In this study the microstructure was analyzed to understand the hydraulic behavior of LBF. LBF mainly comprises 50-50 bentonite sand mixture compacted at a maximum dry density of 1.24 Mg/m^3 . Na-rich bentonite is widely used as backfill material because of its high swelling capacity and low hydraulic conductivity (Kawaragi et al., 2009). However, because of the high compressibility of compacted bentonite materials, it shows

crack during the period of desiccation. These desiccations crack can be reduced by mixing a percentage of silt or clay. The hydraulic behavior of the compacted bentonite was investigated using automated GDS Oedometer. However to explore the reason for which it showed low hydraulic conductivity, it is necessary to visualize the internal structure of the LBF sample. Although the internal porosity of soil can be measured using mercury intrusion porosimetry (MIP) but to visualize the pore structure and to observe the nature of the pore space and geometry in more details, micro-focus X-ray CT is a good option.

X-ray computed tomography (X-ray CT) is a non-destructive technique of determining the microstructure of an object. This technique has been applied in various geotechnical investigations over the last 30 years such as bulk density (Anderson et al., 1990), volumetric water content (Crestana et al., 1984), layer detection (Macedo et al., 1998), porosity (Grevers et al., 1989), pore distribution (Al-Raoush and Willson, 2005), permeability (Ketcham and Carlson, 2001), and desiccation crack on the fine grained soil (Gebrenegus et al., 2011). Additionally, most of the research is focused on coarse grained to medium grained soil. The use of X-ray CT technique on the fine grained soil like bentonite and / bentonite-sand mixture is limited. Although some of the researchers work on the desiccation crack of bentonite clay that developed due to the long term soil-water integration and high compressibility of bentonite clay. According to the authors knowledge, only Hemes et al., 2015 described the microstructural behavior such as porosity, pore size distribution and pore connectivity of

clayey soil (Boom Clay). However they used dry samples, thus the effect of clay water interaction was not observed. Clay water interaction is an important phenomenon for the hydraulic behavior of clayey soil because when water is added to the clayey soil it swells to a great extent by forming a diffuse double layer (DDL) on around each particle. This diffuse double layer minimizes the number and size of pore the pore in the soil mass and successively reduced the permeability of soil. In this study the microstructural behavior of sand, bentonite, bentonite-sand mixtures in both the dry and saturated (LBF) conditions were investigated. Therefore, this study will be a very first attempt to investigate the microstructural behavior of compacted bentonite-sand mixture in relation to saturated conditions.

2 MATERIALS AND METHODS

2.1 Materials

In this study Na-rich Wyoming bentonite and silica sand with a proportion (in weight) of 50 % were used to prepare LBF. The X-ray diffraction (XRD) analysis of Wyoming bentonite showed that the main mineral component is montmorillonite content of 76 %. The particle size of bentonite and sand was determined using scanning electron microscope (SEM) and the result showed that 90 % of the bentonite particles are within the range of 2 to 15 μm , where silica sand includes a particle range of 200 to 600 μm . The oven dried bentonite powder and silica sand were mixed by hand and saturated at a water content of 19 %. The saturated mixture was then compacted into an Oedometer mold to attain a target dry density of 1.24 Mg/m^3 . Afterwards, the LBF samples were used to conduct swelling pressure and one dimensional consolidation test using GDS automated Oedometer. After the one dimensional consolidation test the LBF samples were cut into a propylene tube having diameter of 5.5 m. Propylene tube is advantageous to reduce the loss of moisture content during scanning of the LBF sample. A special sample holder was designed using propylene tube as shown in Figure 1.

2.2 X-ray CT observations

In order to investigate the microstructural behavior of LBF sample, the material used to prepare the LBF samples such as dry sand, bentonite and bentonite-sand mixture were first studied. This preliminary idea on the microstructural behavior of the materials helps to identify the particles in the LBF and the change in microstructure due to the clay-water interaction phenomenon. Therefore three dry samples along with the LBF sample were prepared according to the Table 1. The propylene tube used in the sample holder was filled with the dry materials and compacted by hand to make a compacted mass. It is found that the dry density of sand (S1) is higher than the bentonite (S2). However, the compacted 50-50 dry bentonite-sand mixture gives a moderate value of dry density.

Table 1. Test Scheme for X-ray CT observation

Sample No.	Materials used in the sample	Maximum dry density (Mg/m^3)	Water content (%)
S1	Dry sand	1.65	-
S2	Dry bentonite	1.50	--
S3	Dry bentonite-sand mixture	1.60	--
S4	Saturated bentonite-sand mixtures	1.22	19

Xradia Micro XCT-400 X-ray tomographic microscope located at the University of British Columbia Okanagan (UBCO) was used to acquire the 3D images of the dry materials and distilled water saturated LBF sample (Figure 1). Commercially available propylene tube having diameter of 5.5 mm was used to prepare the sample holder to holds the samples. The advantage of using propylene tube is that it minimizes the loss of water from the saturated LBF during scanning. After placing the samples onto the rotating disk, an X-ray energy of 70 kV with a current of 125 μm were applied to acquire the radiographs of the LBF samples over a rotation from -180° to +180°. The radiographs of the object were acquired based on the attenuation coefficient of the electromagnetic wave reflected by the object. The attenuation coefficient i.e. the X-ray energy absorbed by the object depends on the density of the material (Helliwell et al., 2013). The attenuation coefficient of the acquired images was integrated using backpropagation algorithm to generate 2D reconstructed image slices. Each reconstructed image slices comprises a unit indicates the resolution of the scans. The 3D resolution is termed as the voxel of the image.

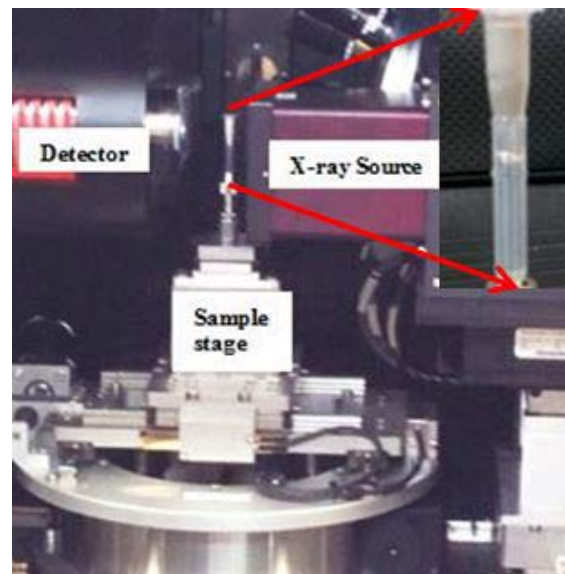
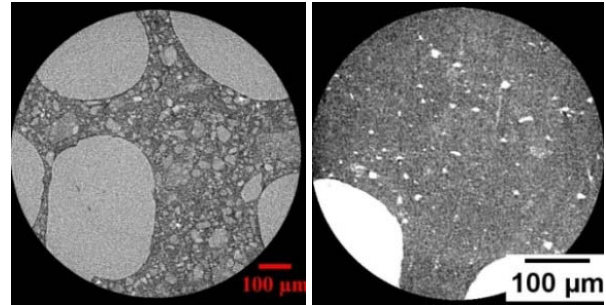


Figure 1. Samples mounted on the rotating disk of Xradia Micro XCT-400

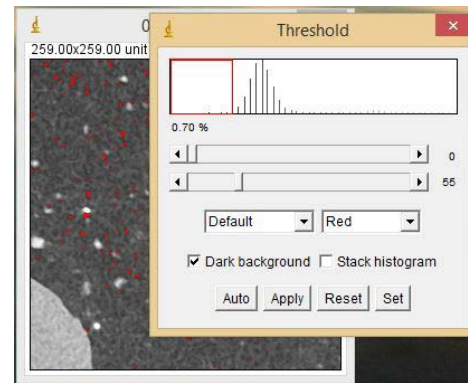
The quality and resolution of the X-ray CT primarily depends on the (i) size of the sample; (ii) distance between the sample and X-ray source; (iii) distance between sample and the detector; and (iv) exposure time for each radiographs (Dhondt et al., 2010). The quality and resolution of the scanned images were adjusted by changing the position of the detector and the X-ray source from the sample holder. High resolution image can be acquired by (i) increasing the distance between the detector and the specimen and (ii) placing the detector and sample closely. However, the image quality found blur, when the detector was placed far away from the specimen. After several trials, it was found that good quality images with a resolution of $1.0695 \mu\text{m}$ can be acquired by placing the detector and X-ray source at a distance of 8 mm and 37 mm from the sample holder, respectively. The size of the sample also affects the quality and resolution of the images as good quality and high resolution images can be acquired with a small size sample. However, small sized sample reflects the local behavior of the sample (Young et al., 2001). Hence, a sample of 5.5 mm diameter was used with the application of region of interest during scanning to ensure high resolution of the larger sized sample. The exposure time required for each radiographs was adjusted according to the image quality during the trial scan. Finally, the sample was scanned to acquire 3200 radiographs with an exposure time of 25 sec. Afterwards the scanned radiographs were reconstructed using XMRReconstructor-Cone Beam Software developed by X-radia.

2.3 Image analysis

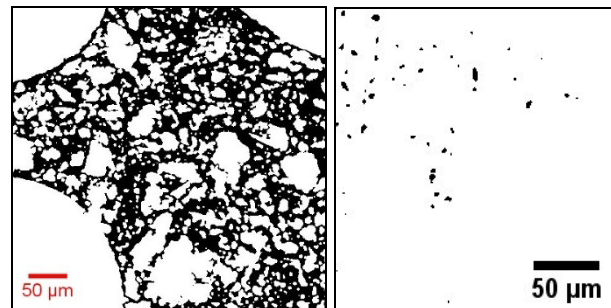
The reconstructed image slices were preprocessed before analyzing microstructural behavior. Initially, the brightness of the scanned images were adjusted (Figure 2a) and cropped to a volume of interest. The images contained speckled noises and it was de-noised using median filter with a radius of 1.35 pixels. Afterward, the de-noised images were segmented to classify (i) the void and particle (Figure 2c); and (ii) different particles (Figure 2d). In the first stage of segmentation, the particle and void were separated with a common mean gray scale known as threshold value. The threshold value was determined using global thresholding technique based on the analysis of histogram of image (Figure 2b). After separating the particles from the void, it was seen that almost all the particles were interconnected with each other, which was further segmented using watershed algorithm. A Gaussian filter with a radius of 1.5 pixels was used before applying watershed algorithm. The segmented images were used for computing microstructural behavior such as porosity, pore size distribution, pore connectivity and absolute permeability.



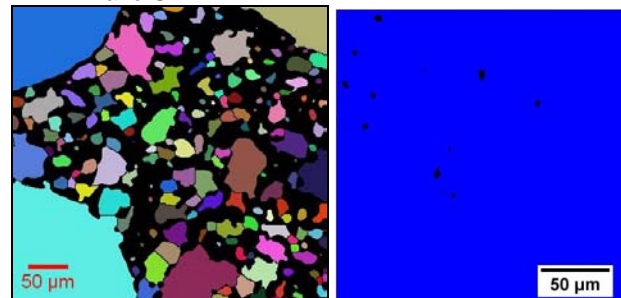
(a) Scanned images of S3 and S4 after adjusting brightness



(b) Application of global thresholding technique



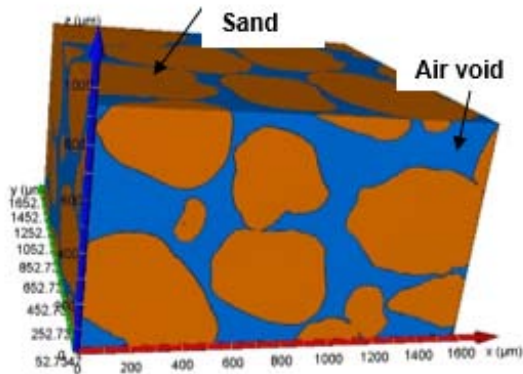
(c) Segmented image after global thresholding of S3 and S4



(d) Segmented image after application of Gaussian filter and watershed segmentation

Figure 2. Preprocessing of scanned images for S3 (dry bentonite-sand mixture) and S4 (LBF)

The segmented images were converted to binary image (0 and 1) to compute the porosity, pore size distribution, pore connectivity and permeability of the samples. An algorithm was developed by the authors to count the black (0) and white (1) voxel present in the binary images. Afterwards the porosity was computed by dividing the black voxel with the total voxel. Another algorithm was developed to compute the pore size distribution. The interconnected pore components were determined using a built in function “connected component analysis” in Avizo Software. The permeability of the samples was computed using Avizo-Xlabsimulation software based on the Darcy’s Law and Stokes theorem with the consideration of incompressible and Newtonian fluid flowing in a steady and laminar manner. Moreover, each voxel of the images were considered as mesh volume and the boundary conditions are (i) no slip occurred in the fluid-solid interface; (ii) the flow is isolated within the system; and (iii) the fluid can freely spread on the face of the sample. The illuminating stream line for the fluid flow through the interconnected pore in dry sand is shown in Figure 3.



3D-microstructure of dry sand

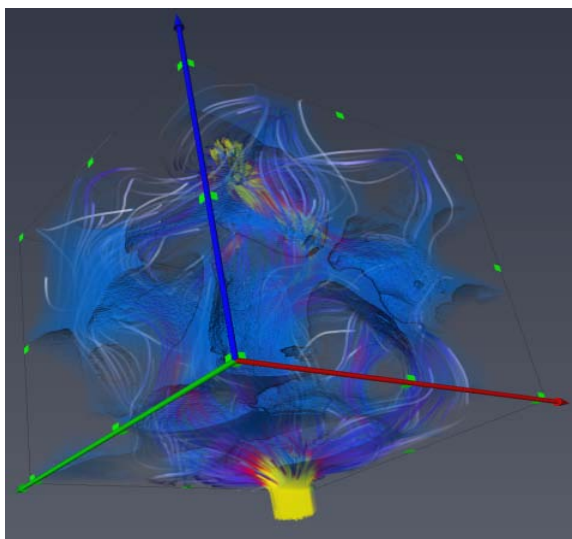


Figure 3. Illuminating stream line of fluid flow through dry sand

3 RESULTS AND DISCUSSIONS

3.1 Porosity and Pore size Distributions

The porosity value calculated from the image analysis (Table 2) showed that the porosity of LBF is very low compared to dry materials. This is due to the formation of DDL around the particles, which results higher swelling pressure. This higher value of swelling pressure reduces the internal pore space.

Figure 4 presents the volumetric pore size distribution of the dry materials and LBF sample. It is observed that approximately 70 % of the pores are less than $100 \mu\text{m}^3$. Almost 50 % pores in both the dry bentonite and bentonite-sand mixtures are greater than $10 \mu\text{m}^3$, while 75 % of pores in LBF are greater than $10 \mu\text{m}^3$.

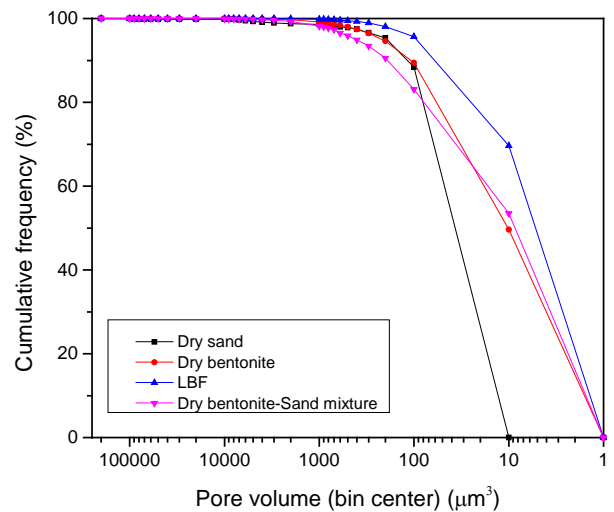


Figure 4. Pore size distribution results

3.2 Pore connectivity

Individual pores are connected with the pore throats, which helps to increase the hydraulic conductivity of soil. The interconnected pore space of LBF sample analyzed using Avizo software is shown in Figure 5. It is observed that most of the connected pore volumes in the LBF samples are very small compared to the dry specimens, which make it less permeable. This is due to the swelling behavior of saturated bentonite. For example, only two pore volume components are larger than $1000 \mu\text{m}^3$ and most of the interconnected pores are within the range of 10 to $100 \mu\text{m}^3$ (Figure 5). It is also observed that the saturated bentonite-sand mixture has no definite flow path to percolate water through it compared to the other dry specimen, where maximum volume of pore components are connected and covered by 100 to greater than $1000 \mu\text{m}^3$ pore volume components (not showed here).

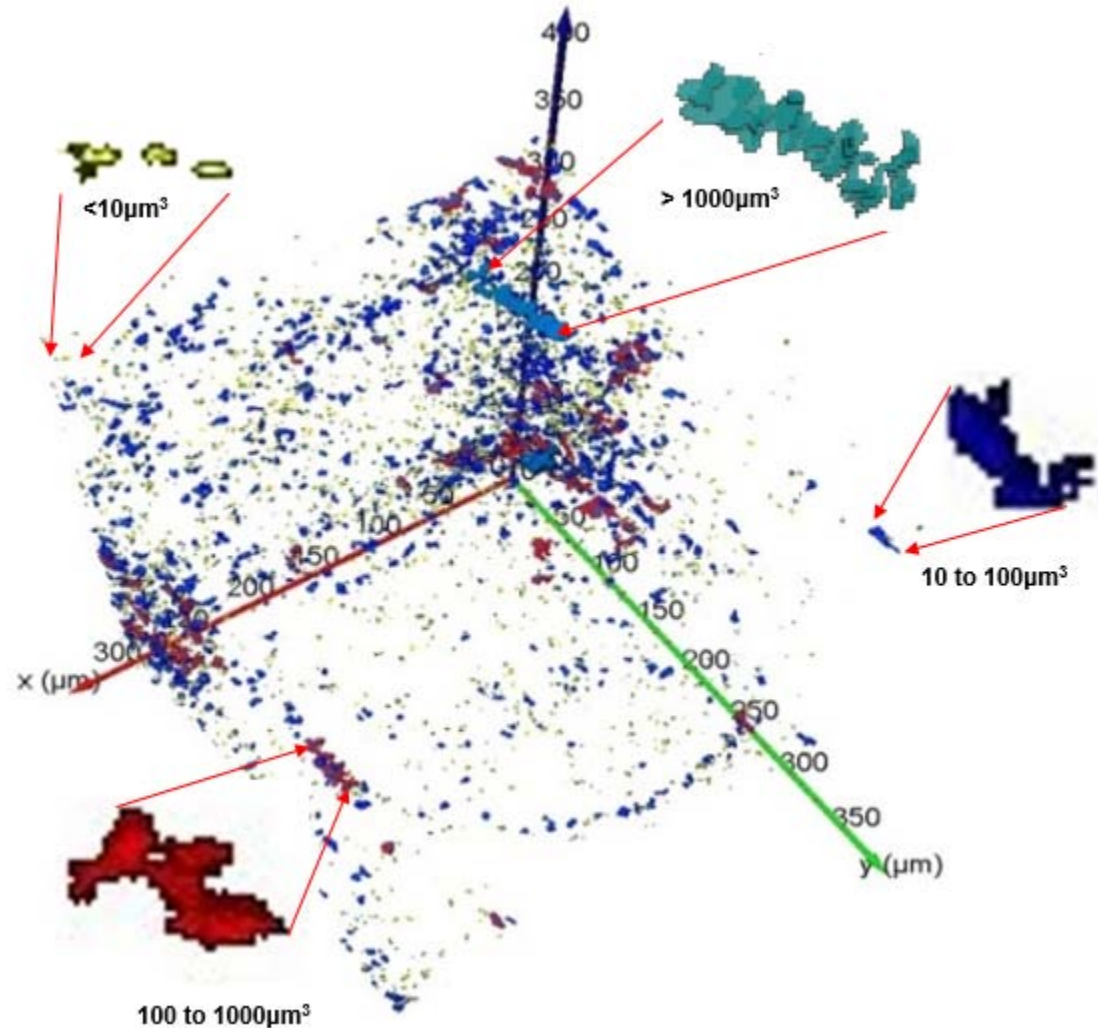


Figure 5. Interconnected pore space showing different sizes of pore volumes of LBF sample

3.3 Permeability

The absolute permeability of small representative samples (400 x 400 x 350 μm) were determined using Avizo software are shown in Table 2. It is observed that the permeability of dry sand, bentonite and bentonite-sand mixture is similar to the typical values shown in Das, 2013. The permeability of the dry materials was very high compared to the DW water saturated LBF. This is due to the formation of bentonite water gel around the particles and development of high swelling pressure based on the DDL theory (Siddiqua et al., 2011).

Table 2. Results of porosity and permeability

Sample	Porosity (%)	Permeability (m ²)
S1	30.47	3.95E-09
S2	68.52	1.73813E-11
S3	29.02	1.58725E-11
S4	0.17	9.37799E-17

4 CONCLUSIONS

In this study the microstructural behaviour of LBF samples were investigated. However, to get preliminary idea on the microstructural properties of material used in the LBF, dry bentonite, sand and bentonite-sand were analysed. Based on the findings of the work, the following conclusion can be made.

- (i) Propylene tube can be used as a sample holder.
- (ii) Good quality image with high resolution was acquired by keeping the distance of X-ray source and detector of 37 mm and 8 mm from the sample.
- (iii) Two algorithms were developed to compute the porosity and pore-size distribution of samples.
- (iv) The results of porosity, pore size distribution and pore connectivity showed that LBF samples

comprises very low porosity and all the pores are in micro level.

- (v) The permeability value found from the X-ray CT analysis

4 REFERENCES

- Al-Raoush, R.I. and Willson, C.S. 2005. Extraction of physically realistic pore network properties from three-dimensional synchrotron X-ray microtomography images of unconsolidated porous media systems. *J. Hydrol.* 300: 44–64. doi:10.1016/j.jhydrol.2004.05.005
- Anderson, S.H., Peyton, R.L. and Gantzer, C.J. 1990. Evaluation of constructed and natural soil macropores using X-ray computed tomography. *Geoderma*, 46: 13–29.
- Baumgartner, P., Priyanto, D., Baldwin, J.R., Blatz, J.A., Kjartanson, B.H. and Batenipour, H. 2008. Preliminary results of one-dimensional consolidation testing on bentonite clay-based sealing components subjected to two pore-fluid chemistry conditions. Nuclear Waste Management Organisation, Toronto. Nuclear Waste Management Organization Report NWMO TR-2008-04. Toronto, Canada.
- Crestana, S., Mascarenhas, S. and Pozzi-Mucelli, R.S. 1984. Static and dynamic 3 dimensional studies of water in soil using computed tomographic scanning. *Int. Cent. Theor. Physics, Trieste* 1–11.
- Das, B.M. 2013. *Advanced soil mechanics*, Fourth Edition. CRC Press.
- Dhondt, S., Vanhaeren, H., Van Loo, D., Cnudde, V. and Inzé, D. 2010. Plant structure visualization by high-resolution X-ray computed tomography. *Trends Plant Sci.* 15: 419–422. doi:10.1016/j.tplants.2010.05.002.
- Gebrenegus, T., Ghezzehei, T.A. and Tuller, M. 2011. Physicochemical controls on initiation and evolution of desiccation cracks in sand-bentonite mixtures: X-ray CT imaging and stochastic modeling. *J. Contam. Hydrol.* 126: 100–12. doi:10.1016/j.jconhyd.2011.07.004.
- Grevers, M.C.J., Jong, E.D. and St. Arnaud, R.J. 1989. The characterization of soil macroporosity with CT scanning. *Can. J. Soil Sci.* 69: 629–637.
- Helliwell, J.R., Sturrock, C.J., Grayling, K.M., Tracy, S.R., Flavel, R.J., Young, I.M., Whalley, W.R. and Mooney, S.J. 2013. Applications of X-ray computed tomography for examining biophysical interactions and structural development in soil systems: a review. *Eur. J. Soil Sci.* 64: 279–297. doi:10.1111/ejss.12028.
- Hemes, S., Desbois, G., Urai, J.L. and Schr, B. 2015. Multi-scale characterization of porosity in Boom Clay (HADES-level, Mol, Belgium) using a combination of X-ray micro-CT, 2D BIB-SEM and FIB-SEM tomography. *Microporous Mesoporous Mater.* 208, 1–20. doi:10.1016/j.micromeso.2015.01.022.
- International Nuclear Societies Council 2012. *Radioactive Waste, Action Plan 1997-98*.
- Ketcham, R.A. and Carlson, W.D. 2001. Acquisition, optimization and interpretation of X-ray computed tomographic imagery: applications to the geosciences. *Comput. Geosci.* 27: 381–400. doi:10.1016/S0098-3004(00)00116-3.
- Macedo, A., Crestana, S. and Vaz, C.M.P. 1998. X-ray microtomography to investigate thin layers of soil clod. *Soil Tillage Res.* 49: 249–253. doi:10.1016/S0167-1987(98)00180-9.
- Siddiqua, S., Blatz, J. and Siemens, G. 2011. Evaluation of the impact of pore fluid chemistry on the hydromechanical behaviour of clay-based sealing materials. *Can. Geotech. J.* 48: 199–213. doi:10.1139/T10-064.
- Statistics Canada 2013. Table 127-0007. Electric power statistics, monthly (Megawatt hour). CANSIM series (database).
- Young, I.M., Crawford, J.W. and Rappoldt, C. 2001. New methods and models for characterising structural heterogeneity of soil. *Soil Tillage Res.* 61: 33–45. doi:10.1016/S0167-1987(01)00188-X.